Research Article | Vol. 7, No. 9 | 1 Sept 2016 | BIOMEDICAL OPTICS EXPRESS 3184

Biomedical Optics EXPRESS

Multimodal optical coherence tomography and fluorescence lifetime imaging with interleaved excitation sources for simultaneous endogenous and exogenous fluorescence

Sebina Shrestha,[1] Michael J. Serafino,[1] Jesus Rico-Jimenez,[1] Jesung Park,[1] Xi Chen,[1] Siqin Zhaorigetu,[2] Brian L. Walton,[2] Javier A. Jo,[1] and Brian E. Applegate[1,*]

[1]*Department of Biomedical Engineering, Texas A&M University, 5045 Emerging Technology Building, College Station, TX, 77843, USA*

[2]*Cardiovascular Experimental Imaging and Therapeutics, Texas Heart Institute, 6519 Fannin St., Houston, TX, 77030, USA*

[*]*apple@tamu.edu*

Abstract: Multimodal imaging probes a variety of tissue properties in a single image acquisition by merging complimentary imaging technologies. Exploiting synergies amongst the data, algorithms can be developed that lead to better tissue characterization than could be accomplished by the constituent imaging modalities taken alone. The combination of optical coherence tomography (OCT) with fluorescence lifetime imaging microscopy (FLIM) provides access to detailed tissue morphology and local biochemistry. The optical system described here merges 1310 nm swept-source OCT with time-domain FLIM having excitation at 355 and 532 nm. The pulses from 355 and 532 nm lasers have been interleaved to enable simultaneous acquisition of endogenous and exogenous fluorescence signals, respectively. The multimodal imaging system was validated using tissue phantoms. Nonspecific tagging with Alexa Flour 532 in a Watanbe rabbit aorta and active tagging of the LOX-1 receptor in human coronary artery, demonstrate the capacity of the system for simultaneous acquisition of OCT, endogenous FLIM, and exogenous FLIM in tissues.

OCIS codes: (110.4500) Optical coherence tomography; (170.2520) Fluorescence microscopy; (170.0110) Imaging systems; (120.3890) Medical optics instrumentation.

References and links

1. Z. G. Wang, D. B. Durand, M. Schoenberg, and Y. T. Pan, "Fluorescence guided optical coherence tomography for the diagnosis of early bladder cancer in a rat model," J. Urol. **174**(6), 2376–2381 (2005).
2. J. A. Jo, J. Park, P. Pande, S. Shrestha, M. J. Serafino, J. J. Rico Jimenez, F. Clubb, B. Walton, L. M. Buja, J. E. Phipps, M. D. Feldman, J. Adame, and B. E. Applegate, "Simultaneous morphological and biochemical endogenous optical imaging of atherosclerosis," Eur. Heart J. Cardiovasc. Imaging **16**(8), 910–918 (2015).
3. Y. Chen, S. A. Yuan, J. Wierwille, R. Naphas, Q. A. Li, T. R. Blackwell, P. T. Winnard, V. Raman, and K. Glunde, "Integrated Optical Coherence Tomography (OCT) and Fluorescence Laminar Optical Tomography (FLOT)," IEEE J. Sel. Top. Quantum Electron. **16**(4), 755–766 (2010).
4. P. C. Ashok, B. B. Praveen, N. Bellini, A. Riches, K. Dholakia, and C. S. Herrington, "Multi-modal approach using Raman spectroscopy and optical coherence tomography for the discrimination of colonic adenocarcinoma from normal colon," Biomed. Opt. Express **4**(10), 2179–2186 (2013).
5. Z. Chen, S. Yang, and D. Xing, "Optically integrated trimodality imaging system: combined all-optical photoacoustic microscopy, optical coherence tomography, and fluorescence imaging," Opt. Lett. **41**(7), 1636–1639 (2016).
6. C. A. Patil, H. Kirshnamoorthi, D. L. Ellis, T. G. van Leeuwen, and A. Mahadevan-Jansen, "A clinical instrument for combined raman spectroscopy-optical coherence tomography of skin cancers," Lasers Surg. Med. **43**(2), 143–151 (2011).
7. B. W. Graf and S. A. Boppart, "Multimodal In Vivo Skin Imaging with Integrated Optical Coherence and Multiphoton Microscopy," IEEE J. Sel. Top. Quantum Electron. **18**(4), 1280–1286 (2012).
8. S. Tang, Y. Zhou, and M. J. Ju, "Multimodal optical imaging with multiphoton microscopy and optical coherence tomography," J. Biophotonics **5**(5-6), 396–403 (2012).

#267650 http://dx.doi.org/10.1364/BOE.7.003184
Journal © 2016 Received 3 Jun 2016; revised 26 Jul 2016; accepted 27 Jul 2016; published 1 Aug 2016

Biomedical Optics EXPRESS

9. S. Liang, A. Saidi, J. Jing, G. Liu, J. Li, J. Zhang, C. Sun, J. Narula, and Z. Chen, "Intravascular atherosclerotic imaging with combined fluorescence and optical coherence tomography probe based on a double-clad fiber combiner," J. Biomed. Opt. **17**(7), 070511 (2012).
10. J. K. Barton, F. Guzman, and A. Tumlinson, "Dual modality instrument for simultaneous optical coherence tomography imaging and fluorescence spectroscopy," J. Biomed. Opt. **9**(3), 618–623 (2004).
11. L. P. Hariri, A. R. Tumlinson, D. G. Besselsen, U. Utzinger, E. W. Gerner, and J. K. Barton, "Endoscopic optical coherence tomography and laser-induced fluorescence spectroscopy in a murine colon cancer model," Lasers Surg. Med. **38**(4), 305–313 (2006).
12. J. M. Jabbour, S. Cheng, B. H. Malik, R. Cuenca, J. A. Jo, J. Wright, Y. S. Cheng, and K. C. Maitland, "Fluorescence lifetime imaging and reflectance confocal microscopy for multiscale imaging of oral precancer," J. Biomed. Opt. **18**(4), 046012 (2013).
13. J. Park, J. A. Jo, S. Shrestha, P. Pande, Q. Wan, and B. E. Applegate, "A dual-modality optical coherence tomography and fluorescence lifetime imaging microscopy system for simultaneous morphological and biochemical tissue characterization," Biomed. Opt. Express **1**(1), 186–200 (2010).
14. M. Gora, K. Karnowski, M. Szkulmowski, B. J. Kaluzny, R. Huber, A. Kowalczyk, and M. Wojtkowski, "Ultra high-speed swept source OCT imaging of the anterior segment of human eye at 200 kHz with adjustable imaging range," Opt. Express **17**(17), 14880–14894 (2009).
15. S. Shrestha, B. E. Applegate, J. Park, X. Xiao, P. Pande, and J. A. Jo, "High-Speed Multispectral Fluorescence Lifetime Imaging Implementation for in Vivo Applications," Opt. Lett. **35**(15), 2558–2560 (2010).
16. H. Y. Lee, P. D. Raphael, J. Park, A. K. Ellerbee, B. E. Applegate, and J. S. Oghalai, "Noninvasive in vivo imaging reveals differences between tectorial membrane and basilar membrane traveling waves in the mouse cochlea," Proc. Natl. Acad. Sci. U.S.A. **112**(10), 3128–3133 (2015).
17. A. Grinvald and I. Z. Steinberg, "On the analysis of fluorescence decay kinetics by the method of least-squares," Anal. Biochem. **59**(2), 583–598 (1974).
18. M. Zuker, A. G. Szabo, L. Bramall, D. T. Krajcarski, and B. Selinger, "Delta-Function Convolution Method (Dfcm) for Fluorescence Decay Experiments," Rev. Sci. Instrum. **56**(1), 14–22 (1985).
19. H. D. Vishwasrao, A. A. Heikal, K. A. Kasischke, and W. W. Webb, "Conformational dependence of intracellular NADH on metabolic state revealed by associated fluorescence anisotropy," J. Biol. Chem. **280**(26), 25119–25126 (2005).
20. D. Magde, G. E. Rojas, and P. G. Seybold, "Solvent dependence of the fluorescence lifetimes of xanthene dyes," Photochem. Photobiol. **70**(5), 737–744 (1999).
21. M. Shiomi and T. Ito, "The Watanabe heritable hyperlipidemic (WHHL) rabbit, its characteristics and history of development: a tribute to the late Dr. Yoshio Watanabe," Atherosclerosis **207**(1), 1–7 (2009).
22. J. Park, P. Pande, S. Shrestha, F. Clubb, B. E. Applegate, and J. A. Jo, "Biochemical characterization of atherosclerotic plaques by endogenous multispectral fluorescence lifetime imaging microscopy," Atherosclerosis **220**(2), 394–401 (2012).
23. D. J. Rader and A. Daugherty, "Translating molecular discoveries into new therapies for atherosclerosis," Nature **451**(7181), 904–913 (2008).
24. H. Chen, S. S. Ahsan, M. B. Santiago-Berrios, H. D. Abruña, and W. W. Webb, "Mechanisms of quenching of Alexa fluorophores by natural amino acids," J. Am. Chem. Soc. **132**(21), 7244–7245 (2010).

1. Introduction

Pathological changes in a tissue are accompanied by alterations in morphology and biochemistry. These alterations are accompanied by changes in the tissue optical properties, e.g. scattering coefficient, distribution of scatterers, absorption coefficient, and fluorescence. Taking advantage of such phenomena, optical imaging systems have been used to establish biomarkers of disease and characterize stages of disease for diagnosis. This "optical biopsy" is particularly advantageous when it is not possible to biopsy the suspect tissue or when the area is so large that sampling error associated with traditional biopsy is unacceptable.

The most complete and presumably reliable optical biopsy would be sensitive to both morphological and biochemical changes. Unfortunately no single optical imaging modality has emerged which can provide both. A promising solution, which has recently garnered a great deal of attention, is to combine two or more modalities such that the product contains the strengths of the constituent modalities. As a combined system, such multi-modal diagnostic tools are capable of interrogating the morphology as well as the biochemistry of tissue. The collective information generated with multi-modal systems has been shown to improve sensitivity and specificity in the analysis of diseased tissues [1–4].

The push to collect both morphological and biochemical information has lead researchers to combine several optical imaging modalities (e.g [5]). They typically combine a modality that largely measures morphology at the tissue or cellular level, e.g. Optical Coherence

Biomedical Optics EXPRESS

Tomography (OCT), confocal reflectance microscopy, or Optical Coherence Microscopy (OCM), with a modality that probes the biochemistry, e.g. fluorescence or Raman microscopy [6–8]. For instance, OCT has been combined with fluorescence imaging for the detection of atherosclerosis [9, 10], colon cancer [11], and early bladder cancer [1]. Reflectance confocal microscopy has been coupled with Fluorescence Lifetime Imaging Microscopy (FLIM) to detect early oral cancer [12] and Raman spectroscopy has been coupled with OCT for discriminating colonic adenocarcinoma [4].

Our group has been investigating multi-modal systems that incorporate OCT and FLIM for the detection of oral cancer and characterization of atherosclerotic plaques [2, 13]. Optical Coherence Tomography (OCT) uses low-coherence interferometry to measure the depth-resolved intensity of light backscattered from the tissue up to a depth of ~2 mm. Changes in the backscattered light intensity generally indicate changes in the refractive index of the tissue which correlates with changes in tissue morphology. The resulting high-resolution cross-sectional and volumetric images thus provide high-fidelity depictions of tissue morphology. Likewise, fluorescence imaging acquires the emission from endogenous fluorescent molecules or exogenous fluorescent markers tagged actively or passively to a biomolecule of interest to generate biochemical maps of the tissue. In our work, we use single photon FLIM with a weak confocal gate; hence the signal is integrated in depth and generates 2-D maps of the biochemistry. The depth over which the signal is integrated in tissue and wavelength dependent, but generally ranges over 200-400 μm from the tissue surface. Together OCT and FLIM can provide biochemical and morphological maps of the tissue at imaging rates compatible with *in vivo* imaging.

As we have noted before [13], a major obstacle to integrating these two modalities is the extreme bandwidth over which the optical system must function. In our prior work, we developed a multimodal system with fluorescence excitation at 355 nm, emission collection bands at 390 ± 20 nm, 452 ± 22.5 nm and 475-850 nm, integrated with a spectrometer based OCT system centered at 830 nm, for a total optical bandwidth of ~500 nm. Here we describe a system that doubles that bandwidth, operating over 355-1360 nm wavelength range or ~1000 nm. The OCT system uses a swept laser source centered at 1310 nm which improves OCT imaging depth. In addition, we have added the capacity to excite fluorescence at 532 nm in order to be sensitive to exogenous molecular contrast agents that can be actively tagged to nonfluorescent biomolecules of interest.

Biomedical Optics EXPRESS

2. Methods

2.1 OCT-FLIM hardware

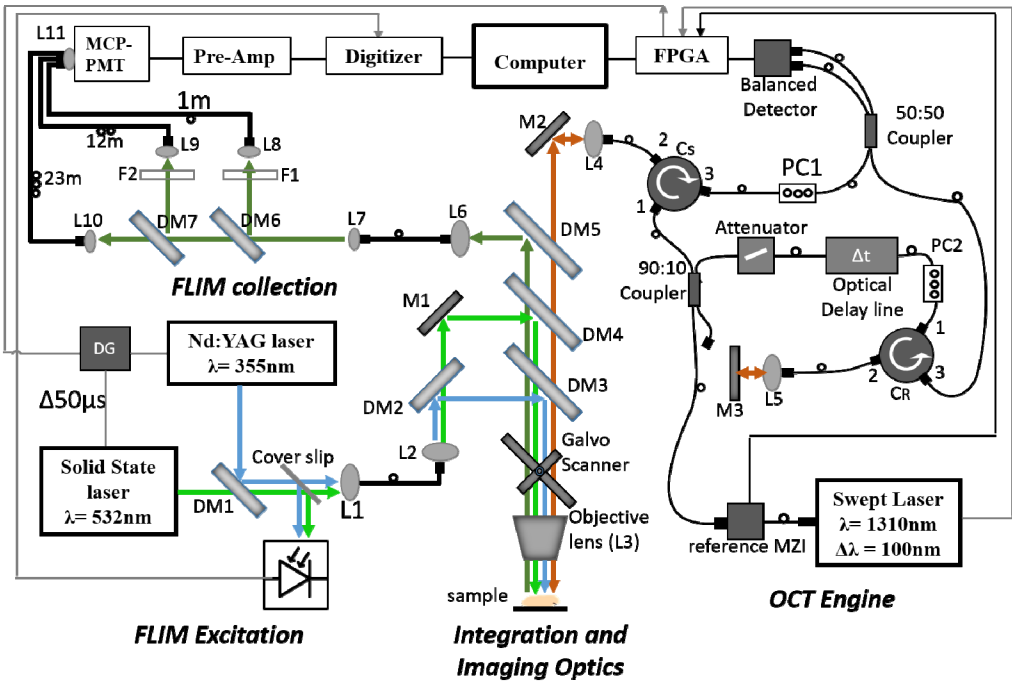

Fig. 1. Schematic of OCT_FLIM system. Green line represents the excitation beam for exogenous FLIM; Blue line is the excitation beam for endogenous FLIM; Olive line is the emission; Maroon line is the beam for OCT. Note that overlapping co-linear beams are shown as parallel lines for clarity. The thin grey line is the trigger path. DM1-DM7: Dichroic Mirrors, L1-L10: Lenses, M1-M2:Mirror, PC1-PC2:Polarization controller, F1-F2:Longpass and bandpass filters, MCP-PMT-Multi-channel plate photo multiplier tube, Pre-Amp-Pre-amplifier, MZI-Mach Zehender Interferometer, FPGA- Field Programmable Gate Array, DG-Delay Generator.

The developed system, shown schematically in Fig. 1, can be logically divided into four subsystems, OCT engine, FLIM excitation, FLIM collection, and Integration and Imaging Optics. The OCT and FLIM were optically and electronically synchronized such that the multimodal images were collected simultaneously and co-registered. The pulsed output of the 532 nm and 355 nm lasers were interleaved such that alternate pulses excited endogenous and exogenous fluorescence. The free-space optical paths in the system are color-coded in Fig. 1 as: Green - excitation light for exogenous fluorophores, Blue - excitation light for endogenous fluorophores, Olive – fluorescence emission, Maroon –1310 ± 60 nm OCT beam path. The black lines indicate optical fibers and thin gray lines indicate connections for triggering. Details of the subsystems follow.

OCT engine

A 1310 nm swept source laser (ESS320024-00, Exalos, Switzerland) with uni-directional sweep rate of 50 kHz (bi-directional, 100 kHz), tuning bandwidth of 100 nm and coherence length of 6 mm in air was used as the source for the OCT system. The laser output first entered a commercial Mach-Zehnder type interferometer (MZI) (INT-MZI-1300, Thorlabs, USA), whose interference signal provided a wavelength reference for spectral calibration and linearization [14]. Only 5% of the laser output was used for the MZI. The remaining 95% entered a 90:10, 2x2 single-mode fiber coupler (10202A-90-APC, Thorlabs, USA). The 10%

Biomedical Optics EXPRESS

output was directed to the reference arm of the OCT interferometer. The reference arm consisted of a fiber variable optical attenuator (VOA50-APC, Thorlabs, USA) followed by an optical delay line (ODL)(VDL-001-35-60-FC/APC/APC-SS, General Photonics, USA) with a range of 0-600 ps. The output from the ODL port 1 of a circulator (CIR1310PM-APC, Thorlabs, USA), exited the fiber pigtail of port 2 and was collimated by a lens (L5) before being focused onto a mirror placed at a distance such that the optical pathlength in air was matched between the reference and sample arms. Light reflected from this mirror reentered port 2 and was recombined with the sample arm light via port 3 and a 50:50 2x2 single-mode fiber coupler (NPMC-22-F-13-50/50-FC/APC, General Photonics, USA). The 90% output was directed into port 1 of a circulator. The exit from port 2 was collimated and sent into the Integration and Imaging Optics (discussed below). The light reentering port 2 from the sample exited port 3 and was recombined with the reference light via the 50:50 coupler, the outputs of which entered a InGaAs balanced photodetector (WL-BPD600MA, Weiserlab, Germany). The interferometric signal was digitized at 400 MS/s with a National Instruments FPGA (NI PXIe 7966, National Instruments, USA) based digitizer (NI 5772, National Instruments, USA). Custom LabVIEW software was written to control the imaging system and process all data. The measured signal-to-noise of the system, corrected for a perfect reflector was 107dB with a 3 dB sensitivity roll-off of 2.75 mm.

FLIM excitation

A frequency tripled (355 nm) Q-switched Nd:YAG laser (SPOT-10-50-355, Elforlight Ltd., England), pulsed at 10 kHz with width of 2ns and maximum energy of 5 μJ, was used as the excitation source for the endogenous fluorophores in the tissue. A 532 nm solid state laser (1Q532-2, CryLas GmbH, Germany) with a maximum repetition rate of 10 kHz and pulse energy of 3.2μJ was utilized to excite the exogenous fluorescent dye tagged to the receptor of interest. The pulses from the 355 and 532 nm lasers were interleaved such that the effective pulse rate for FLIM was 20 kHz with every other pulse exciting endogenous or exogenous fluorescence. The requisite trigger delays were created using a delay generator (P400, Highland Technology Inc., USA). The output from both lasers was spatially combined using a dichroic mirror, DM1 in Fig. 1, (425DCXR, Chroma Technology, USA) that reflected 355 nm light and passed 532 nm light. A thin quartz coverslip reflected a small portion of light onto a photodiode (DET36A, Thorlabs, USA) to generate a 20 kHz trigger for digitizing the fluorescence signal. These excitation beams were coupled into a multimode fiber with a core diameter of 50 μm (FG050UGA, Thorlabs, USA) to deliver light to the *Integration and Imaging Optics*.

Integration and imaging optics

The FLIM excitation exiting the multimode fiber was reimaged onto the sample using lenses L2 and the Objective lens after passing through a series of dichroic mirrors. The 355 nm and 532 nm excitation beams were separated with a dichroic mirror, DM2 (470DCXR, Chroma Technology, USA). 355 nm light was reflected with DM2 and DM3 (365DCLP, Chroma Technology, USA) that transmitted everything above 365 nm. Similarly, 532 nm light was reflected with a notched dichroic mirror, DM4 (NFD01-532, Semrock, USA) such that the beam travelled together with the 355 nm and 1310 nm beams. All three beams were directed to a galvanometer scanner (6220H, Cambridge Technology, USA) used to scan the three coaligned beams in the x,y plane of the sample. An achromatic lens (NT64-837, Edmund optics, USA) served as the objective, providing a maximum field of view of 16 mm by 16 mm, and a lateral resolution of 34 μm for OCT and 120 μm for FLIM. Note, the resolution of OCT and FLIM can be tuned independently because they do not share the same tube lens (L2 and L4, in Fig. 1) which allows for different magnification for both. The objective was designed for 193 - 1000 nm, however we found that it had good performance out to 1350 nm. The ~1 mm chromatic shift from the objective enabled the system to be optimally setup such

Biomedical Optics EXPRESS

that the FLIM excitation was focused near the surface of the tissue sample while the OCT light was focused ~1 mm inside of the tissue. The fluorescene emission was reflected via DM5 (BLP01-980R, Semrock, USA) into a 200 μm core diameter multimode fiber (BFL22-200, Thorlabs, USA), which delivered the light to the multispectral *FLIM collection* system described below. Backscattered nearIR light from the OCT illumination passed back through the series of dichroic mirrors and reentered the circulator (Cs) at port 2.

FLIM collection

Following the basic architecture in [15], a combination of dichroic mirrors, DM6 (R405lp, Chroma Technology, USA) and DM7 (FF520Dio2, Semrock, USA), and bandpass filters, F2 (FF01-390/40, Semrock, USA) and F3 (FF01-494_41, Semrock, USA) were used to separate the fluorescence emission into three spectral bands: 390 ± 20 nm (channel 1), 494 ± 20.5 nm (Channel 2) and > 542 nm (Channel 3). Emission in channel 1, 2 and 3 were coupled into multimode fibers (BFL22-200, Thorlabs, USA) with a core size of 200 μm and varying lengths of 1 m, 11.5 m and 24 m, respectively. The difference in length between the consecutive channels provided an interval of ~60 ns between their time-resolved fluorescence emissions at the detector. All 3 fibers were collimated onto the 11 mm diameter quartz window of Multi-channel plate photomultiplier tube (MCP-PMT) with 150 ps rise time (R3809U-50, Hamamatsu, Japan). Output of the MCP-PMT was amplified using a high-bandwidth pre-amplifier (C5594, Hamamatsu, Japan) and was digitized at sampling rate of 4 GS/s using a PCI-ADC card (CS14G8 CobraMax, GaGe, USA). The digitizer was triggered at 20 kHz with pulses from a photodiode excited by the interleaved excitation laser pulses.

OCT-FLIM synchronization

Custom software written in LabVIEW was developed to synchronize and control the subsystems. The 50 kHz sweep trigger from the swept-laser source was used as the master clock for synchronization. The sweep trigger was connected to the trigger input of the NI 5772 digitizer adapter module. The PXIe7966 FPGA then initiated data acquisition and outputted clock and trigger signals to the PXI-6713 analog output card to control the two mirrors of the galvanometer scanner and the delay generator. The delay generator provided two output triggers for each trigger received from the PXI-6713 analog output card. One trigger was routed to the 355 nm laser, and the other to the 532 nm laser. A temporal shift of 50 μs was added to the trigger signal for the 532 nm laser in order to time interleave the 355 and 532 nm pulses. The FLIM signal digitizer was triggered by the pulse from the photodiode activated by the excitation beams. The pulse energy of the FLIM excitation lasers at the sample was 1.3 μJ (355 nm) and 0.9 μJ (532 nm) with a pulse repetition rate of 10 kHz (20 kHz interleaved).

Since the spatial resolution differed between OCT and FLIM and the fluorescence from the two excitation sources were collected serially, some care had to be taken in choosing the scanning and sampling parameters to ensure co-registration. Given that the lateral resolution for OCT was 34 μm and 120 μm for FLIM, the FLIM pixels needed to be acquired approximately 3.5 times slower to achieve the same samples/resolution as OCT. However, the maximum pulse rate of our 532 nm source was 10 kHz, hence we acquired FLIM pixels 5 times slower than OCT. With the OCT and FLIM frequencies fixed at 50kHz and 10kHz, respectively, the raster scanning scheme was organized as shown in Fig. 2.

Figure 2(a) depicts the raster scan on the sample and identifies Frame 0 and 1 referenced in 2b. The arrows represent the movement of the collinear OCT and FLIM beams steered by the galvo mirrors during imaging. The trigger diagrams in Fig. 2(b) only shows 10 OCT samples 2 FLIM pixels per frame for brevity. The signals are described as follows from the bottom of Fig. 2(b). The OCT sweep trigger (Fig. 2(bi)) is generated by the swept laser source and acts as the master clock. Fig. 2(bii) is the internal trigger logic on the OCT FPGA/digitizer omitting triggers during the flyback of the galvo mirrors. In general the OCT

Biomedical Optics EXPRESS

signal was sampled at 2 samples per resolution or every 17 µm. A 10 kHz trigger is generated by the FPGA (Fig. 2(biii)) and sent to a delay generator (DG). The 10 kHz trigger signal is then used to trigger the 355 nm laser (Fig. 2(biv)) and the 532 nm after a 50 µs delay (Fig. 2(bv)). The result is a 20 kHz pulse train that is partially reflected into a photodiode (PD). The output of the photodiode is then used to trigger the FLIM digitizer (Fig. 2(bvi)). The 10 kHz trigger rate for each FLIM excitation laser leads to a sampling rate of approximately 1.4 samples per resolution or every 85 µm in the fast axis. In the slow axis the sampling is nominally the same as for OCT, every 17 µm. In general, we resample/spatially average the FLIM data so that the sampling is 2 samples per resolution or 60 µm in both dimensions. As described, this scheme provides for spatial averaging of ~3 along the slow axis. Obviously one could alter the scan parameters to also allow for spatial averaging in the fast axis if there was a need to improve the signal to noise ratio.

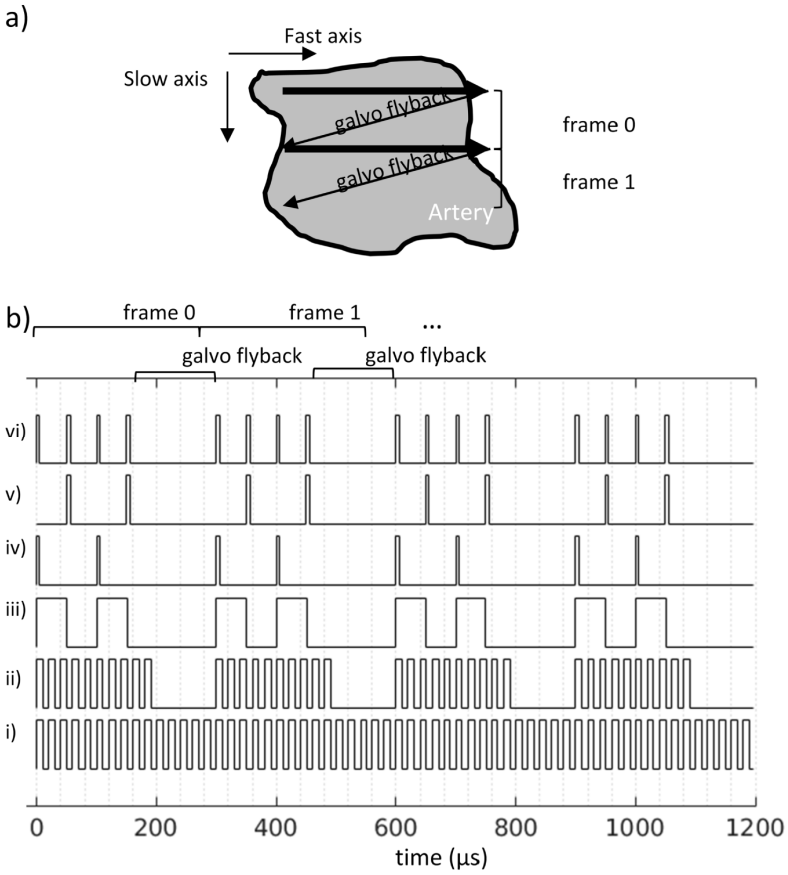

Fig. 2. a) cartoon showing the fast and slow axes of a raster scan along with frame labels referenced in the trigger diagrams of b). The arrows represent the movement of the collinear OCT and FLIM beams steered by the galvo mirrors during imaging. b) Trigger diagrams for signals used to sample OCT and FLIM. The temporal sampling rates are fixed according to sweep rate of the OCT swept source (50 kHz) and the pulse repetition rate of the FLIM excitation lasers (10 kHz). For brevity only 10 OCT lines and 2 FLIM pixels are acquired per frame in this illustration. i) sweep trigger from swept source acts as the master clock. ii) internal trigger logic on FPGA/digitizer that omits the triggers during the galvo flyback. iii) 10 kHz digitial signal output by the analog output card and sent to a delay generator. iv) undelayed trigger signal from delay generator used to trigger 355 nm laser. v) 50 µs delayed trigger signal used to trigger 532 nm laser. vi) photodiode signal used to trigger FLIM digitizer.

Biomedical Optics EXPRESS

Processing of the spectral interferograms to generate OCT images proceeded as described in [16]. Briefly, the spectral interferograms were calibrated by using the phase of the Hilbert transform of the signal from the reference MZI (see Fig. 1). A numerical phase correction was added to compensate for dispersion in the optical system before calculating the discrete inverse Fourier transform. The magnitude with the negative path lengths discarded was the A-line. Galvo scanning of the laser in the x,y plane enabled the acquisition of cross-sectional (B-scan) and volumetric images.

The time resolved fluorescence measurements were processed using an iterative nonlinear least squares exponential model [17]. In the case of endogenous tissue fluorescence, a bi-exponential model was used. A single exponential model was used for exogenous fluorescence. The decay for each channel was deconvolved with the measured instrument response specific to each channel. The absolute intensity was calculated by integrating the observed fluorescence decay. Since emission generated by 355 nm excitation illuminated all three channels, the absolute intensity in each channel was normalized by the sum of the absolute intensity in all channels. For the human coronary artery tissues described below the signal to noise ratio in the 3rd channel was very low, hence only channels 1 and 2 were included in the normalization. The average florescence lifetime was computed using the deconvolved temporal decay. The resulting values were assembled into 2-D maps of absolute intensities, normalized intensities and average lifetime [13].

2.2 Visualization

In order to visualize the multidimensional information, the fluorescence-derived maps were projected onto the surface of the corresponding co-registered OCT volume image. The surface of the OCT volume was determined by finding the first index in the A-line whose intensity is greater than or equal to the mean plus 2-3 standard deviations of the mean of the A-line. The standard deviation threshold was manually adjusted for each OCT volume as needed to obtain satisfactory surface detection. Median filters were used for smoothing the detected surface in both x and y directions. Rendering of the overlaid version of OCT/FLIM images was accomplished using a custom 3-D visualization tool using VTK and developed in C++.

2.3 Nonspecific tagging of Watanabe heritable hyperlipidemic (WHHL) rabbit aorta

A section of WHHL aorta was acquired postmortem from a rabbit euthanized due to deteriorating health. The sample was cleaned with PBS and opened longitudinally with surgical scissors. It was then divided in two, with the first sample (sample 1) ~10 mm long and the second sample (sample 2) ~4 mm long. Both were washed with PBS for fifteen minutes, changing the PBS every five minutes. A solution of 1% of Bovine Serum Albumin (BSA) (BP671-1, Fisher Scientific, USA) and 0.1% of Tween-20 (BP337-500, Fisher Scientific, USA) in PBS was prepared. Sample 2 was incubated for one hour in 5 µl of Alexa Fluor 532 goat anti-rabbit IgG (A-11009, Life Technologies, USA) diluted with 1 ml of the BSA, Tween-20, and PBS solution. BSA prevents nonspecific binding and Tween-20 enhances the permeability of the tissue. After incubation, sample 2 was thoroughly washed with PBS. Both samples were then imaged with OCT/FLIM system. The pulse energy at the sample was 40 nJ at 355 nm and 504 nJ at 532 nm. The pulse energy of the 355 nm laser was reduced from what we typically use for endogenous fluorescence measurements in order to make the emission intensity due to 355 nm excitation roughly equivalent to the emission intensity due to 532 nm excitation. This was necessary since the system uses one detector for all of the emission channels.

2.4 LOX-1 tagging of postmortem human coronary arteries

Human coronary artery obtained from an adult autopsy case was trimmed to remove the unwanted fats and muscles surrounding the artery. The tissue was then cleaned with PBS and

Biomedical Optics EXPRESS

cut open longitudinally. Tissue was washed with PBS for fifteen minutes by changing the solution every five minutes. Sample was imaged using the OCT-FLIM system. The pulse energy of the 355 nm laser was reduced to ~31.23 nJ at the sample while that of the 532 nm laser was maintained at ~374 nJ.

Sample was again washed thoroughly with PBS as mentioned before. Subsequently, the samples were incubated with 1% of goat serum (G9023-5ML, Sigma-Aldrich Co.,LLC, USA) in PBS for an hour, followed by a 15 minute PBS wash. A solution of 3% of BSA and 0.1% of Tween-20 in PBS was prepared. Sample was incubated overnight with 20µl of rabbit anti-LOX-1 antibody (ab60178, Abcam, USA) mixed in 1ml of the BSA-Tween20 solution. Sample was washed and imaged with the system. Sample was incubated for 2 hours in a mixture of 5µl of Alexa Fluor 532 goat anti-rabbit IgG and 1ml of the BSA-Tween20 solution. After incubation, sample was washed with PBS thoroughly and imaged. The imaged tissue was then placed in 10% Formalin and processed for histopathological slides.

3. Results

3.1 System validation with capillary tubes filled with fluorophores

In order to assess the performance of the OCT/FLIM system, we imaged 3 parallel, coplanar quartz capillary tubes, each filled with a different fluorophore and submerged in diluted milk as a scattering medium. 1,4-bis(5-phenyloxazol-2-yl) benzene (POPOP) and Nicotinamide Adenine Dinucleotide (NADH) fluoresce efficiently at 400 nm and 500 nm, respectively, when excited at 355 nm. Rhodamine 6G emits at wavelengths greater than 550 nm when excited with 532 nm light. Solutions of POPOP in ethanol, NADH in Phosphate Buffer Saline (PBS), and Rhodamine6G in ethanol were prepared to have concentrations of 50 µM, 1 mM and 2.8 µM, respectively. These concentrations were chosen to ensure acquisition of emissions with comparable intensities while using the same amplification on the PMT. The capillary tubes had 0.3 mm inner diameter and 0.4 mm outer diameter. Their ends were carefully sealed before being submerged in the scattering medium. This sample was then raster scanned with a field of view of 2.4 mm x 2.4 mm.

Figure 3(a) is the set of intensity and lifetime maps (60x60 pixels) derived from the fluorescence emission data measured on the capillary tube sample. Any fluorescence from the scattering media that was below 22.5% of the maximum was set to zero. Upon 355 nm excitation, POPOP exhibited the strongest emission in channel 1, while NADH exhibited the strongest emission in channel 2. Neither POPOP nor NADH exhibited emission when excited with 532 nm light. Rhodamine6G emitted when excited with 355 or 532 nm, exhibiting strong emission in channel 3. These observations were consistent with what was expected based upon the known excitation/emission spectra of all three fluorophores. The mean ± standard deviation of the average lifetime of POPOP, NADH and Rhodamine6G calculated over each capillary tube upon 355 nm excitation was 1.26 ± 0.04 ns, 0.42 ± 0.03 ns and 3.51 ± 0.13 ns, respectively. The average lifetime of Rhodamine6G was 3.59 ± 0.06 ns when excited with 532 nm. The literature values for the average lifetime of POPOP. NADH, and Rhodamine 6G are 1.38 ± 0.01 ns [18] 0.44 ns [19] and 3.99 ± 0.03 ns [20], respectively.

Figure 3(b) is the 2.4 x 2.4 x 0.98 mm OCT volume image of the tissue phantom fused with the coregistered FLIM images where the FLIM is projected onto the surface of the OCT volume. The dark circular regions depict the cross-section of the capillary tubes surrounded by the scattering media. The diameter of the capillary tubes measured from the OCT volume image was 0.4 mm, in good agreement with the known diameter. The centers of the capillary tubes were ~290 µm below the surface of the scattering medium. The FLIM map depicted here is the combination of the channel 2 and channel 3 lifetime maps.

Biomedical Optics EXPRESS

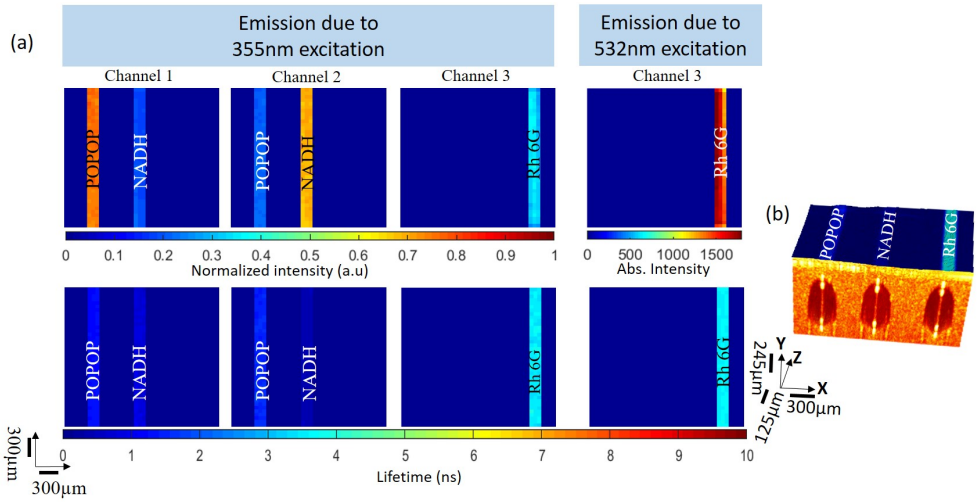

Fig. 3. (a) FLIM images of capillary tubes filled with POPOP, NADH and Rhodamine 6G, submerged in a scattering tissue phantom. As expected POPOP has maximum peak in channel 1, NADH in channel 2 and Rhodamine 6G in channel 3. Rhodamine 6G emitted when excited with both 355 nm or 532 nm. The average lifetimes derived from the time-resolved images where: POPOP (1.26 ± 0.04ns), NADH (0.42 ± 0.03 ns) and Rhodamine (3.51 ± 0.13 ns and 3.59 ± 0.06 ns when excited with 355 and 532nm respectively). (b) OCT volume (2.4 x 2.4 x 0.98 mm) image of the submersed capillary tubes overlaid with the combined lifetime data from channel 2 and channel 3.

3.2 WHHL rabbit aorta imaging

Initial testing of the system for simultaneous endogenous and exogenous fluorescence signals measurement was performed on an *ex vivo* non-specifically tagged aorta of a WHHL rabbit. WHHL rabbits have a genetic mutation that produces Low-density Lipoprotein (LDL) receptor deficiency similar to human familial hyperlipidemic disorder. Likewise they exhibit a lipoprotein metabolism similar to humans [21]. This condition makes them prone to developing atherosclerotic plaques.

Two aorta samples were obtained. Sample 2 was tagged with Alexa Fluor 532, while sample 1 served as an untagged control. Each scan of the sample produced an OCT volume, fluorescence emission intensity and lifetime maps from 3 channels due to 355 nm excitation and 1 channel (channel 3) due to 532 nm excitation. WHHL rabbit endogenous emission (355 nm excitation) in channel 3 was negligible, hence the endogenous emission maps for channel 3 were not plotted in the figures below.

Biomedical Optics EXPRESS

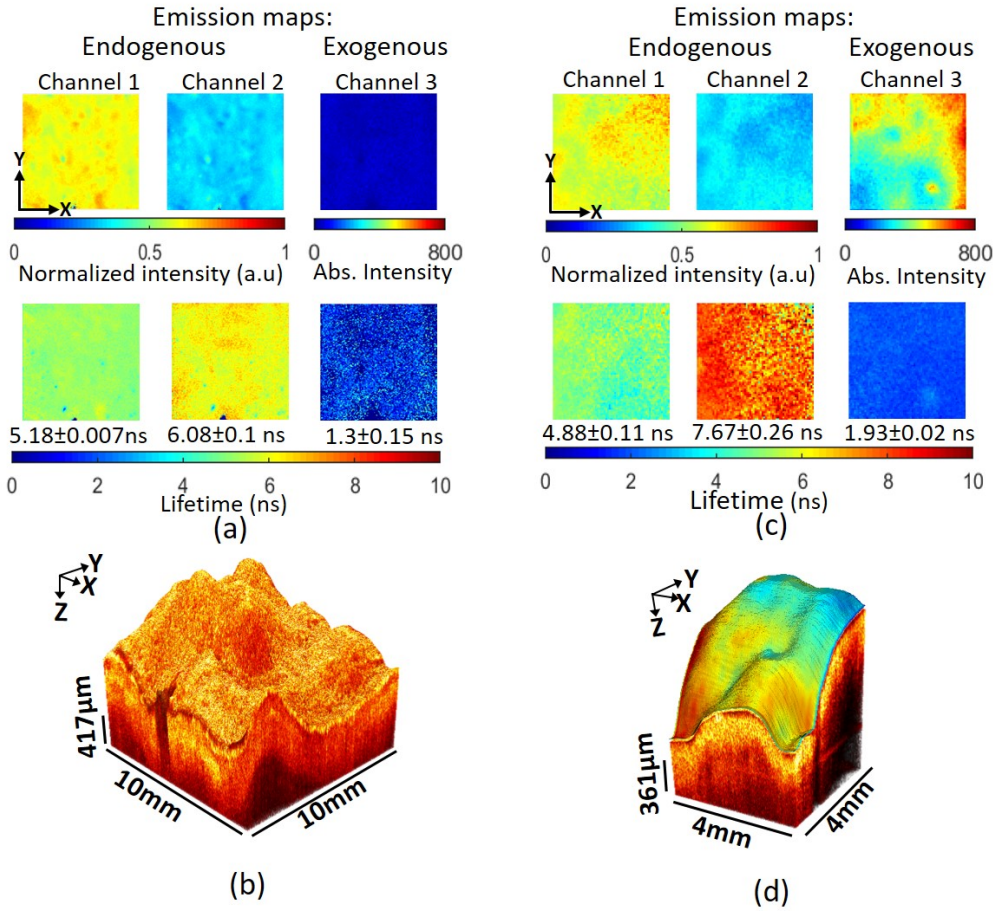

Fig. 4. Results Watanabe rabbit aorta samples. (a) FLIM maps of Watanabe rabbit aorta (Sample 1). Intensity and lifetime maps in channel 1 and 2 due to 355nm laser excitation are consistent with collagen fluorescence. In this unstained sample low/no signal in channel 3 indicates a lack of endogenous fluorescence upon 532 nm excitation. (b) Volumetric OCT image collected simultaneously showing a single bright homogenous layer characteristic of pathological intimal thickening (PIT). (c) FLIM images of Watanabe rabbit aorta tagged with Alexa Fluor 532 (Sample 2). Maps in channel 1 and 2 due to 355nm laser are consistent with collagen fluorescence. The lifetime measured in channel 3, 1.93ns, is consistent with the Alexa Fluor 532 fluorescent tag. (d) OCT volume overlaid with the intensity map of exogenous emission. A single bright homogenous layer in the OCT volume image is characteristic of PIT.

Figure 4 shows the OCT and FLIM images obtained from samples 1 and 2. Results in Fig. 4(a) show that the intensity in channel 1 was higher than in channel 2 for sample 1, suggesting a strong contribution of collagen fluorescence to the signal. Lifetimes in channels 1 (5.18 ± 0.07 ns) and 2 (6.08 ± 0.1 ns), reported as the mean and standard deviation over the entire map, are also consistent with a strong fluorescence contribution from collagen. Normalized intensity maps of sample 2, in Fig. 4(c), showed a pattern of endogenous emission similar to sample 1. While channel 1 exhibited a similar lifetime (4.88 ± 0.11 ns) as in sample 1, channel 2 exhibited a much longer lifetime, 7.67 ± 0.26 ns. This shift [22] suggested the presence of lipid deposits scattered throughout the tissue in addition to collagen. Channel 3 in each figure is the intensity and lifetime of the tissue sample upon excitation at 532 nm. The lack of signal in channel 3 for sample 1 (Fig. 4(a)) was consistent with the absence of Alexa Fluor 532 as well as endogenous fluorescence. In contrast, sample

Biomedical Optics EXPRESS

2 (Fig. 4(c)) exhibited significant intensity indicating the presence of the Alexa Fluor 532. The relatively uniform lifetime map (1.93 ± 0.02 ns) is consistent with our measurements of unconjugated Alexa Fluor 532, 2.55 ± 0.06 ns. The difference between the conjugated and unconjugated lifetime is likely simply due to the change in environment brought on by covalently binding the fluorophore.

Both OCT volumes in Fig. 4(b) and Fig. 4(d) exhibit a single bright homogenous layer characteristic of pathological intimal thickening (PIT). Taken together with the FLIM information the plaque in sample 1 is a high-collagen PIT and the plaque in sample 2 is a high-collagen and high-lipid PIT.

3.3 Human coronary artery imaging

A similar experiment was also conducted on postmortem human coronary artery, which was tagged with Alexa Fluor 532 specifically targeting the LOX-1 receptors. LOX-1 are abundant in the endothelial cell of the intima and are the receptors for oxidized LDL (ox-LDL). The binding of LOX-1 and ox-LDL initiates formation of lipid-rich foam cells on the artery [23].

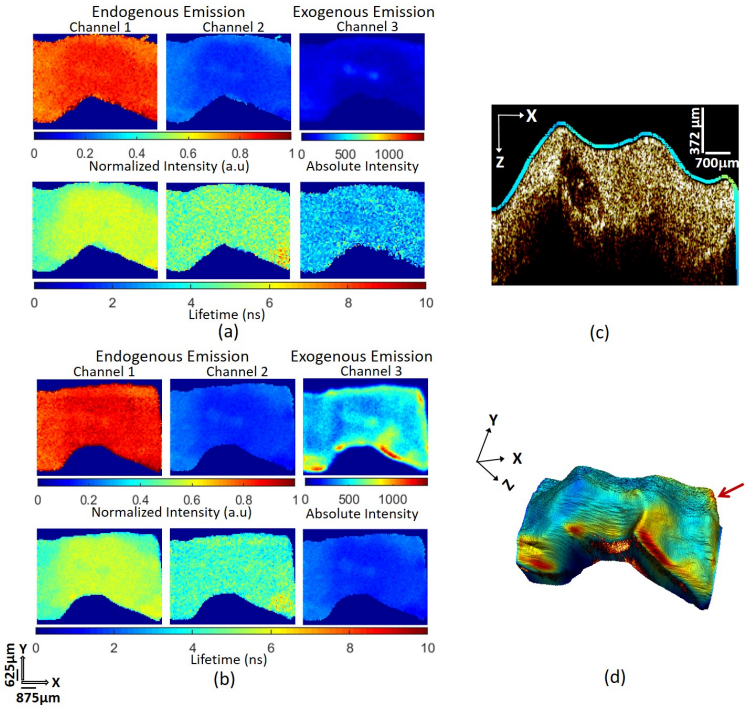

Fig. 5. Results obtained by imaging human coronary artery before and after tagging with Alexa Fluor 532. (a) FLIM maps of the artery before tagging. (b) FLIM maps of the tissue after tagging. Intensity in channel 1 in both figures is higher than that in channel 2, suggesting a strong contribution of collagen fluorescence in the signal. Comparison of the absolute emission intensities in channel 3 of these figures indicate successful tagging of Alexa Fluor 532. Average lifetime of the tissue in channel 3 before tagging is 3.07 ± 0.26 ns. Channel 3 average lifetime after tagging (1.91 ± 0.03 ns) is similar to the lifetime of nonspecific tagged Alexa Fluor 532 in the Watanbe rabbit sample. (c) Representative cross-sectional image from the OCT volume overlaid with the exogenous emission map. The OCT image is consistent with pathological intimal thickening. The dark region (center-left) is a calcified area. The fluorescence intensity is consistent with a relatively uniform expression of LOX-1 except on the right corner of the tissue. (d) OCT volume image overlaid with the exogenous FLIM emission map. Red arrow indicates the approximate location of the cross-sectional image shown in (c).

Biomedical Optics EXPRESS

Figure 5(a) and Fig. 5(b) show the FLIM images obtained from the same sample before and after tagging it with anti-LOX-1 conjugated with Alexa Fluor 532, respectively. In both sets of FLIM maps, intensity is higher in channel 1 than in channel 2, indicating the presence of collagen. Lifetimes in channels 1 (5.32 ± 0.15 ns before tagging and 5.22 ± 0.14 ns after tagging) and channel 2 (4.82 ± 0.19 ns before tagging and 4.28 ± 0.17 ns after tagging) are similar before and after tagging and consistent with collagen fluorescence. The channel 3 intensity map in Fig. 5(a) (prior to tagging) shows some endogenous emission from the tissue due to excitation at 532 nm. The average lifetime for the emission was 3.07 ± 0.26 ns. After tagging (Fig. 5(b)), the intensity is significantly higher and the average lifetime is reduced to 1.91 ± 0.03 ns. Higher intensity and shorter lifetime in channel 3 are consistent with fluorescence emission from LOX-1 receptors tagged with Alexa Fluor 532. The Alexa Fluor 532 lifetime is comparable to what was measured in the nonspecifically tagged Watanabe rabbit sample (1.93 ± 0.02 ns) and again slightly lower than that of Alexa Flour 532 in solution (2.55 ± 0.06 ns). Quenching of Alexa Flour fluorescence is known to occur upon conjugation [24] so the reduction in lifetime from that observed in solution is not unexpected.

Figure 5(c) is a representative cross-sectional image from the 3D OCT volume overlaid with the channel 3 (exogenous) intensity map, Fig. 5(d). The cross-section was extracted along the X-axis at the point indicated approximately by the red arrow on Fig. 5(d). The OCT cross-section is consistent with pathological intimal thickening with a region (center-left) showing a calcified necrotic core. The fluorescence intensity indicates relatively low expression of the LOX-1 receptor except on the right corner, where the intensity is ~30-50% higher than the rest of the cross-section. A similar observation of the image in Fig. 5(d) indicates that LOX-1 is fairly evenly expressed across the tissue except for a few “hot” spots that appear red in the image.

4. Discussion

Results from the tissue phantom revealed good agreement between measured fluorescent lifetimes and literature values in all spectral windows and with both excitation wavelengths. The rhodamine 6G capillary exhibited fluorescence from both 355 nm and 532 nm excitation. The measured lifetime from both agreed to within the standard deviation of the measurements. Time interleaving of the pulses from the two excitation lasers enabled serial acquisition of FLIM image pixels. Judicious choices of the sampling in the image acquisition ensured that the FLIM images are coregistered with each other and the OCT volume image.

The WHHL rabbit results demonstrated that the general approach, i.e. interleaved excitation sources, can effectively be used to detect both endogenous and exogenous fluorescence. The WHHL plaque had essentially no endogenous fluorescence upon 532 nm excitation, hence the nonspecifically tagged exogenous fluorophore could be detected free of background. In contrast, the human coronary artery plaque had weak endogenous fluorescence at 532 nm that was overpowered by the fluorescence from the LOX-1 labeled fluorophore. In our experience so far, in the context of atherosclerosis, the endogenous background fluorescence at 532 nm excitation is very weak. However, future work looking at a wider variety of plaque phenotypes or other samples types may exhibit appreciable endogenous background signal. In those cases, several approaches may be taken to separate the endogenous and exogenous fluorescence. For instance, if there is fluorescence in channel 3 from both 355 nm and 532 nm excitation, as was the case for the tissue phantom (rhodamine 6G), then the signal from 355 nm excitation could be used to estimate and remove the endogenous background signal. Similarly, the measured channel 3 lifetime from 355 nm excitation along with the known lifetime of the exogenous tag could be used as inputs into a multiexponential decay model to extract the magnitudes of the signals. Both approaches require that the emission from the exogenous fluorophore is negligible at 355 nm excitation as was the case for Alexa Flour 532.

Biomedical Optics EXPRESS

In all, the newly developed imaging system performed well and certainly adequate for our needs, nevertheless it is worth pointing out several issues related to this design that may be addressed in future work. The choice of dichroic mirrors is critical to the system performance. They need to have high-reflectivity for the excitation wavelengths and relatively sharp transitions to high-transmission of visible and near-IR beams. Ideally, a single dichroic mirror with high notch reflectivity for both 355nm and 532nm could reduce the transmission/reflectance losses and the complexity of the OCT and FLIM common path. Due to unavailability of such part at a reasonable cost, two dichroic mirrors were introduced to the common path to reflect the excitation beams, adding transmission losses on the path. In general, we chose to bias the system towards the fluorescence system. In other words, if a compromise was necessary we chose the optimal solution for the fluorescence system. The OCT system has a fairly high sensitivity, well over 100 dB. Given that fact, we analyzed that we could afford to sacrifice a few dB of OCT signal to gain fluorescence photons. As a consequence, we lost a few dB of OCT signal due to optical losses and generated ghost images above and below the main OCT image. The optical pathlength between the ghost images is such that it is relatively easy to spatially separate them as was done for the images shown here. However, if we were to become interested in imaging more weakly scattering samples, the ghost images could be overlapped. This could be remedied by reworking the system of dichroic mirrors to bias the system more toward the OCT system at the expense of fluorescence signal.

Another design choice was to use the same detector for endogenous and exogenous fluorescence emission. As a consequence, emission from different fluorophores needs to be comparable in order to adequately utilize the dynamic range of the detector/digitizer. We accomplished this in the experiments above by tuning the output power of the two excitation laser sources. If the strengths of the endogenous and exogenous flourophores are significantly different, we may pay a price in the signal-to-noise ratio using this approach because one excitation source would need to be heavily attenuated. However, there are other solutions where we could avoid this compromise. For instance, we could use a power supply for the PMT that could be modulated at the laser repetition frequency thus enabling different gain for exogenous (355 nm excitation) and endogenous (532 nm excitation) fluorescence. Alternatively, we could separate channel 3 onto an additional detector which would obviously allow different gain for channels 1-2 and 3. Both solutions would add significant cost and complexity to the system.

It may appear from the complexity of Fig. 1 that miniaturization for *in vivo* applications would be very challenging. However, much of the complexity comes from the "FLIM collection" optics. Since that portion is fiber coupled, it can remain remote from any miniature/hand-held imaging optics. In fact, only DM3 (in Fig. 1) would need to be with the miniature imaging optics in a bulk imaging system. Using specialty fibers to combine the OCT illumination with the UV fluorescence excitation can further simply the system. We are currently using this approach to develop a catheter-based system for intravascular imaging. Similar strategies could be used to develop a miniature bulk optic system for clinical applications.

In conclusion, we have developed and validated a multimodal OCT and FLIM imaging system capable of measuring fluorescence emission upon excitation at 355 nm and 532 nm. Collection of the emission was over 3 channels, 390 ± 20 nm, 494 ± 20.5 nm and > 542 nm. Using this system, we were able to uniquely separate endogenous and exogenous fluorescence due to Alexa Fluor 532 in a WHHL rabbit aorta and human coronary artery atherosclerotic plaque.

Funding

National Heart, Lung, and Blood Institute (NHLBI) (1R01HL111361)